

Cluster structure of ^{21}Ne and ^{21}Na

R. Bijker

*Instituto de Ciencias Nucleares, Universidad Nacional Autónoma de México,
Apartado Postal 70-543, 04510 Cd. de México, México*

F. Iachello

*Center for Theoretical Physics, Sloane Laboratory, Yale University,
New Haven, CT 06520-8120, U.S.A.*

Abstract

We study the cluster structure of ^{21}Ne and ^{21}Na within the framework of the cluster shell model (CSM) and show that they have a complex cluster structure with the coexistence of a $^{20}\text{Ne}+n$, $^{20}\text{Ne}+p$ structure and a $^{19}\text{Ne}+2n$, $^{19}\text{F}+2p$ structure. Seven rotational bands are identified in ^{21}Ne and four in ^{21}Na and assigned to single-particle cluster states, single-hole cluster states and vibrational states. The single-particle states are associated with the $^{20}\text{Ne}+n$ and $^{20}\text{Ne}+p$ cluster structure, while the single-hole states are associated with the $^{19}\text{Ne}+2n$ and $^{19}\text{F}+2p$ structure.

Keywords: Cluster model, Alpha-cluster nuclei, Algebraic models

1. Introduction

Cluster structures in light nuclei were suggested in 1965 by Brink [1] and later extensively investigated within the framework of the Brink-Bloch model [2, 3, 4] for all nuclei with $N = Z$ composed of k α -particles to be denoted henceforth by $k\alpha$ nuclei. Several geometric configurations were analyzed and it was concluded that the geometric structure of the ground state of ^8Be ($k = 2$) is a dumbbell (\mathcal{Z}_2 symmetry), of ^{12}C ($k = 3$) is a triangle (\mathcal{D}_{3h} symmetry) and of ^{16}O ($k = 4$) is a tetrahedron (\mathcal{T}_d symmetry). These three structures have been recently re-analyzed [5, 6, 7, 8, 9], especially in ^{12}C , in view of recent experimental data on the rotational structure of the ground state band and of the so-called Hoyle band [10, 11, 12, 13]. In the Brink model [2], also ^{20}Ne ($k = 5$), ^{24}Mg ($k = 6$), and ^{28}Si ($k = 7$) were analyzed with suggested configurations for ^{20}Ne of a bi-pyramid (\mathcal{D}_{3h} symmetry), for ^{24}Mg a rhombic bi-pyramid (\mathcal{D}_{2h} symmetry) and for ^{28}Si a double-winged structure with either \mathcal{D}_{2h} or \mathcal{D}_{2d} symmetry. For

Email addresses: bijker@nucleares.unam.mx (R. Bijker),
francesco.iachello@yale.edu (F. Iachello)

these nuclei several other structures have been suggested, in particular for ^{20}Ne a body-centered distorted tetrahedron [14] and a $^{16}\text{O}+\alpha$ structure [15]. Very recently, we have provided evidence [16], on the basis of an extensive analysis of data accumulated in the last 50 years, that the cluster structure of ^{20}Ne appears to be a bi-pyramid thus confirming the suggestion of Brink [2].

An important question is the extent to which cluster structures survive the addition or subtraction of particles. We denote these structures by $k\alpha + x$ nuclei, where $x = 1, 2, \dots$, is the number of additional particles. These structures were originally suggested by von Oertzen [17, 18, 19, 20]. The simplest case is $x = 1$. In a previous publication, one of us (F.I.) with Della Rocca analyzed the structure of ^9Be and ^9B as $^8\text{Be}+n$ and $^8\text{Be}+p$ [9] by using the so-called cluster shell model (CSM) [21, 22]. In another publication we analyzed the structure of ^{13}C as $^{12}\text{C}+n$ [23]. In view of recent experimental data in ^{21}Ne [24] combined with old measurements [25], we analyze in this paper the cluster structure of ^{21}Ne and show that this nucleus has a complex structure with the coexistence of particle and hole states with cluster structure $^{20}\text{Ne}+n$ and $^{19}\text{Ne}+2n$. We also analyze the structure of the mirror nucleus ^{21}Na and show that it can be described by the coexistent cluster structures $^{20}\text{Ne}+p$ and $^{19}\text{F}+2p$. The approach of this paper generalizes the previous approach to $k\alpha+x$ nuclei [9, 21] to more complex situations.

In a major development of the last few years, large scale shell model calculations have become feasible. In particular the development of the SDPF interaction [26] has allowed large scale calculations of s-d shell nuclei. The analysis of experimental data presented here gives the opportunity to test whether cluster features can be obtained from large shell model calculations. A comparison between shell model and cluster interpretation will be presented elsewhere [27].

The structure of this paper is as follows. In Sect. 2, we briefly review the cluster structure of ^{20}Ne . In Sect. 3, we assign states in ^{21}Ne to rotational bands. These assignments are for most cases identical to those given in Ref. [24]. However, differences occur for two bands which have a major effect on the interpretation of the cluster structure of ^{21}Ne . In Sect. 4, we provide an interpretation of the observed rotational bands in terms of the cluster shell model (CSM) [9], summarize our assignments, interpret those in terms of clustering and compare with other assignments and models. In Sect. 5, we analyze the available experimental information in ^{21}Ne on electromagnetic transition rates and moments and compare with cluster calculations. In Sect. 6, we discuss the structure of ^{21}Na and compare it with that of ^{21}Ne . Finally, Sect. 7 contains a summary and conclusions.

2. Cluster structure of ^{20}Ne

The starting point of our study is the cluster structure of ^{20}Ne . This structure has been very recently analyzed [16]. Ground state properties of ^{20}Ne appear to be well described by a bi-pyramidal configuration, α - ^{12}C - α , with D_{3h}

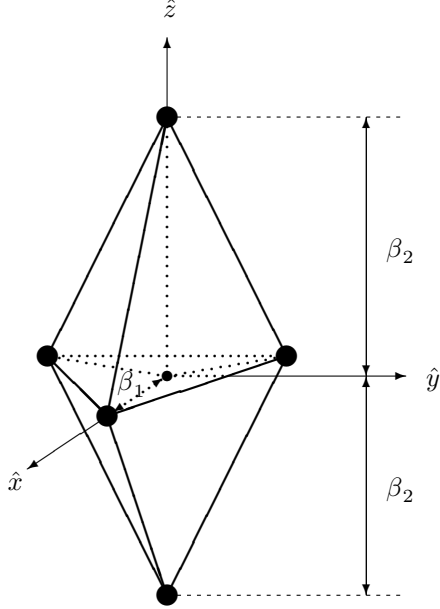


Figure 1: A bi-pyramidal structure with \mathcal{D}_{3h} symmetry.

symmetry, Fig. 1. The coordinates $(r_i, \theta_i, \varphi_i)$ of the five constituent α -particles are

$$\begin{aligned}
 (r_1, \theta_1, \varphi_1) &= (\beta_1, \frac{\pi}{2}, 0) , \\
 (r_2, \theta_2, \varphi_2) &= (\beta_1, \frac{\pi}{2}, \frac{2\pi}{3}) , \\
 (r_3, \theta_3, \varphi_3) &= (\beta_1, \frac{\pi}{2}, \frac{4\pi}{3}) , \\
 (r_4, \theta_4, \varphi_4) &= (\beta_2, 0, -) , \\
 (r_5, \theta_5, \varphi_5) &= (\beta_2, \pi, -) .
 \end{aligned} \tag{1}$$

Assuming a gaussian distribution for the density of the α -particles,

$$\rho_\alpha(\vec{r}) = \left(\frac{\alpha}{\pi}\right)^{3/2} e^{-\alpha r^2} , \tag{2}$$

we have an overall density

$$\begin{aligned}
 \rho(\vec{r}) &= \frac{1}{5} \left(\frac{\alpha_1}{\pi}\right)^{3/2} \sum_{i=1}^3 \exp \left[-\alpha_1 (\vec{r} - \vec{r}_i)^2 \right] \\
 &+ \frac{1}{5} \left(\frac{\alpha_2}{\pi}\right)^{3/2} \sum_{i=4}^5 \exp \left[-\alpha_2 (\vec{r} - \vec{r}_i)^2 \right] .
 \end{aligned} \tag{3}$$

In the calculation of [16], it was assumed that all α -particles are identical with $\alpha_1 = \alpha_2 = \alpha = 0.53 \text{ fm}^{-2}$ obtained from the r.m.s. radius $\langle r^2 \rangle_\alpha^{1/2} = 1.674(12) \text{ fm}$ of the free α -particle. All properties of the ground state of ^{20}Ne can then be determined in terms of two parameters β_1 and β_2 . A fit to the elastic form factor in electron scattering gives $\beta_1 = 1.82 \text{ fm}$, $\beta_2 = 3.00 \text{ fm}$, from which one calculates the r.m.s. radius $\langle r^2 \rangle^{1/2} = 2.89 \text{ fm}$, the intrinsic quadrupole moment $Q_0 = 52.5 \text{ efm}^2$ and the quenched moment of inertia $I/m = 97.6 \text{ fm}^2$ [16]. We note incidentally here that while the density Eq. (3) describes well the r.m.s. radius and intrinsic quadrupole moment, it does not describe well the moment of inertia and a quenched value had to be used in [16]. This may be due to the neglect of Pauli exchange contributions which make the cluster structure tighter than that given in Eq. (3) (see the comparison between quenched and unquenched values in Section 3.4 of [16]).

The excitation spectrum of ^{20}Ne consists of the vibrational states of the bi-pyramidal configuration [16]. There are $15 - 6 = 9$ vibrations, three singly degenerate and three doubly degenerate. The species of these vibrations, their characterization and numbering are given in [16]. In characterizing the representations we can use the representations of the group D_{3h} which is the symmetry group of the bi-pyramid of Fig. 1. The energy levels of ^{20}Ne can then be written as those of a symmetric top (rotational part) and in the harmonic approximation (vibrational part) as

$$E([v], K, L) = E_0 + B_{x[v]}L(L+1) + [B_z - B_x]_{[v]}K^2 + \sum_{i=1}^6 \omega_i v_i. \quad (4)$$

where $[v] \equiv [v_1, v_2, v_3, v_4, v_5, v_6]$, L is the angular momentum and K the projection on the intrinsic axis (z -axis in Fig. 1). The vibrational and rotational parameters of ^{20}Ne are summarized in Table 1. Here Γ denotes the representations of D_{3h} , K the projection of the angular momentum on the z -axis and P the parity.

In the following sections, we make also reference to the cluster structure of ^{19}Ne and ^{19}F . These nuclei can be viewed either as a hole in the structure of ^{20}Ne , or equivalently as a bi-pyramid in which one α particle on the z -axis of Fig. 1 is replaced by ^3H (in ^{19}F) or ^3He (in ^{19}Ne), in which case the symmetry of the cluster is reduced from D_{3h} to D_3 , with composition $\alpha - ^{12}\text{C} - ^3\text{H}$ or $\alpha - ^{12}\text{C} - ^3\text{He}$.

3. Structure of ^{21}Ne

Extensive sets of experimental data have been accumulated in the last 50 years. We use here the recent compilation of Firestone [25]. In order to compare with theoretical models we first make assignments of the observed energy levels into rotational bands characterized by a value of J and K . The rotational bands

Table 1: Summary of rotational and vibrational parameters in ^{20}Ne [16].

	Γ	K^P	ω (MeV)	B (keV)
g.s.	A'_1	0^+	0.00	212
v_1	A''_2	0^-	5.52	137
v_2	A'_1	0^+	6.72	127
v_3	A'_1	0^+	7.19	130
v_4	E'	1^-	8.59	134
		2^+	8.53	112
v_5	E'	1^-	8.42	147
		2^+	8.71	130
v_6	E''	1^+	9.68	124
		2^-	4.10	145

are analyzed with the formula

$$E_{rot}(\Omega, K, J^P) = \varepsilon_\Omega + B_\Omega [J(J+1) - b_\Omega K^2 + a_\Omega (-1)^{J+1/2} (J + \frac{1}{2}) \delta_{K,1/2}] \quad (5)$$

where Ω labels the rotational bands in ^{21}Ne , ε_Ω is the intrinsic energy, B_Ω is the inertial parameter $B_\Omega = \hbar^2/2I$, a_Ω the decoupling parameter and b_Ω has contributions from both the symmetric top [16] and the Coriolis term [28]

$$b_\Omega = \frac{B_{x[v]} - B_{z[v]}}{B_{x[v]}} + 2 \cong 1, \quad (6)$$

since the first term is ~ -1 in ^{20}Ne as given in Eq. (30) of [16]. In the following analysis we take $b_\Omega = 1$.

3.1. Assignments of states to bands

We identify bands by the value of K^P and the energy of the $J^P = K^P$ state in the band. States are assigned on the basis of their energy, their electromagnetic transition rates and their branching ratios when available, and of their spectroscopic factors in (d, p) and (p, d) reactions. For the low-lying states the assignments are straightforward, but at higher excitation energy they are rather difficult since there are several states with the same spin and parity. We have been able to identify seven bands as shown in Table 2 and Fig. 2. The superscript a in Table 2 denotes states with no spin assignment in [24].

4. Cluster interpretation of rotational bands

In order to classify the single particle intrinsic states, Ω , we use the cluster shell model (CSM) [21].

Table 2: Rotational bands in ^{21}Ne

$K^P(E_{\text{exc}})$	J^P	E_{exp}	E_{th}
$3/2^+(0)$	$3/2^+$	0	0
	$5/2^+$	351	690
	$7/2^+$	1746	1656
	$9/2^+$	2867	2898
	$11/2^+$	4433	4416
	$(13/2^+)$	6448	6120
	$(15/2^+)$	9857	8280
$1/2^-(2789)$	$1/2^-$	2789	2789
	$3/2^-$	3664	3473
	$5/2^-$	3884	3813
	$7/2^-$	5334	5409
	$9/2^-$	6033	6021
	$(11/2^-)$	7961	8529
	$(13/2^-)$	9401	9413
	$(15/2^-)$	11984	12834
$1/2^+(2794)$	$1/2^+$	2794	2794
	$3/2^+$	4684	4675
	$5/2^+$	3736	3680
	$7/2^+$	7982	8069
	$9/2^+$	6267	6278
$5/2^+(4526)$	$5/2^+$	4526	4526
	$(7/2^+)$	5431	5443
	$9/2^+$	6554	6622
	$(11/2^+)$	8240	8063
	$(13/2^+)$	9700	9766
$1/2^-(5690)$	$1/2^-$	5690	5690
	$3/2^-$	4725	4725
	$(5/2^-)$	8264	8071
	$7/2^-$	5818	5820
$3/2^+(5549)$	$3/2^+$	5549	5549
	$(5/2^+)$	5773	5849
	$(7/2^+)$	6263	6269
	$9/2^+$	6853	6809
$3/2^+(5822)$	$3/2^+$	5822	5822
	$(5/2^+)$	6174	6112
	$(7/2^+)$	$(6412)^a$	6518
	$(9/2^+)$	7044	7040

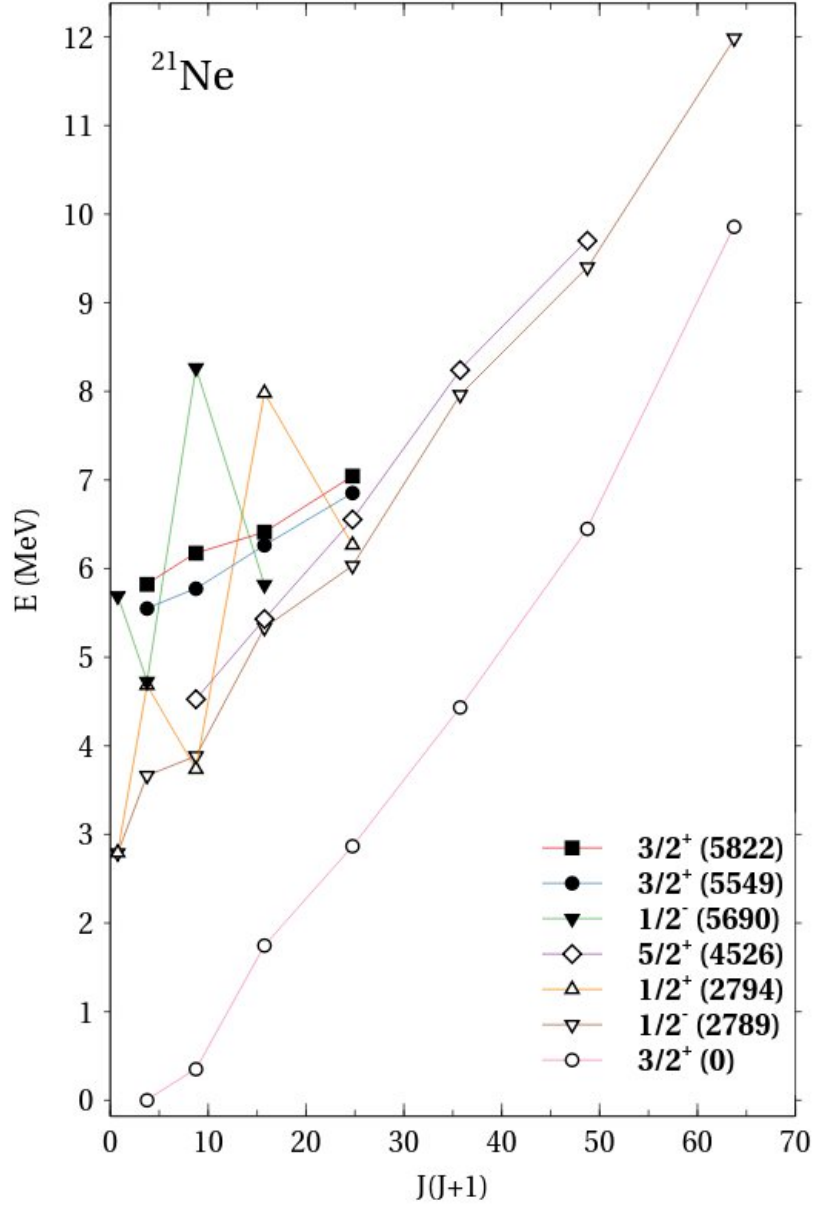


Figure 2: Energies of assigned states in ^{21}Ne to rotational bands as a function of $J(J+1)$.

4.1. Cluster shell model

In the CSM, intrinsic states in ^{21}Ne are calculated by solving the Schrödinger equation

$$H = \frac{\vec{p}^2}{2m} + V(\vec{r}) + V_{so}(\vec{r}) , \quad (7)$$

in the potential generated by the appropriate geometric configuration. For the bi-pyramidal structure of Fig. 1, the potential is given by [21]

$$\begin{aligned} V(\vec{r}) = & -V_1 \sum_{\lambda\mu} f_{\lambda}^{(1)}(r) Y_{\lambda\mu}(\theta, \phi) \sum_{i=1}^3 Y_{\lambda\mu}^*(\theta_i, \phi_i) \\ & -V_2 \sum_{\lambda\mu} f_{\lambda}^{(2)}(r) Y_{\lambda\mu}(\theta, \phi) \sum_{i=4}^5 Y_{\lambda\mu}^*(\theta_i, \phi_i) , \end{aligned} \quad (8)$$

where

$$\begin{aligned} f_{\lambda}^{(1)}(r) &= e^{-\alpha_1(r^2+\beta_1^2)} 4\pi i_{\lambda}(2\alpha_1\beta_1 r) , \\ f_{\lambda}^{(2)}(r) &= e^{-\alpha_2(r^2+\beta_2^2)} 4\pi i_{\lambda}(2\alpha_2\beta_2 r) , \end{aligned} \quad (9)$$

and the spin-orbit potential by

$$\begin{aligned} V_{so}(\vec{r}) = & V_{1,so} \sum_{\lambda\mu} \left(-2\alpha_1 f_{\lambda}^{(1)}(r) + \frac{\lambda}{r^2} f_{\lambda}^{(1)}(r) + \frac{2\alpha_1\beta_1}{r} f_{\lambda+1}^{(1)}(r) \right) \\ & \times \frac{1}{2} \left[Y_{\lambda\mu}(\theta, \phi)(\vec{s} \cdot \vec{l}) + (\vec{s} \cdot \vec{l}) Y_{\lambda\mu}(\theta, \phi) \right] \sum_{i=1}^3 Y_{\lambda\mu}^*(\theta_i, \phi_i) \\ & + V_{2,so} \sum_{\lambda\mu} \left(-2\alpha_2 f_{\lambda}^{(2)}(r) + \frac{\lambda}{r^2} f_{\lambda}^{(2)}(r) + \frac{2\alpha_2\beta_2}{r} f_{\lambda+1}^{(2)}(r) \right) \\ & \times \frac{1}{2} \left[Y_{\lambda\mu}(\theta, \phi)(\vec{s} \cdot \vec{l}) + (\vec{s} \cdot \vec{l}) Y_{\lambda\mu}(\theta, \phi) \right] \sum_{i=4}^5 Y_{\lambda\mu}^*(\theta_i, \phi_i) . \end{aligned} \quad (10)$$

The values of α_1 and α_2 that appear in f_{λ} are not the same as those appearing in the density, since they are obtained by convoluting the density with the α -nucleon interaction as discussed in Eq. (13) of [21]. In both equations we have allowed for the possibility of a different interaction of the nucleon with the α -particles in the xy -plane and with those along the z axis ($\alpha_1 \neq \alpha_2$).

The intrinsic states in the potential of Eqs. (8-10) are characterized by the value of the projection K of the angular momentum of the single particle on the intrinsic z axis, $\langle j_3 \rangle$, and the parity P . A calculation of the single-particle levels in a potential with parameters $V_1 = 5.4$ MeV, $V_{1,so} = 5.4$ MeVfm², $\alpha_1 = 0.0679$ fm⁻², $V_2 = 24.5$ MeV, $V_{2,so} = 24.5$ MeVfm², $\alpha_2 = 0.0679$ fm⁻² at the values of the deformation parameters $\beta_1 = 1.80$ fm, $\beta_2 = 3.00$ fm of ^{20}Ne [16] gives the results in the left column of Fig. 3. The calculation has been carried out in the Z_2 basis using a model space with 10 oscillator shells, $\nu = 0.1833$ fm⁻²

and $\hbar\omega = 15.2$ MeV. In this figure, both the intrinsic energies from the $^{20}\text{Ne}+n$ threshold, denoted by ε'_K in this article, and those relative to the energy of the $K^P = 3/2^+$ intrinsic state at $\varepsilon'_K = -7.22$ MeV, denoted by ε_K in this article, are given, as well as the decoupling parameters a_Ω calculated accordingly to

$$a_\Omega = - \sum_{nlj} (-1)^{j+1/2} \left(j + \frac{1}{2}\right) \left| c_{nlj,1/2}^\Omega \right|^2, \quad (11)$$

where c_{nljm}^Ω are the expansion coefficients of the intrinsic wave functions in the spherical basis

$$|\chi_\Omega\rangle = \sum_{nljm} c_{nljm}^\Omega |nljm\rangle. \quad (12)$$

The decoupling parameter only contributes to $K = 1/2$ bands. The relation between ε_K and ε'_K is

$$\varepsilon_K = \varepsilon'_K - \varepsilon'_{K^P=3/2^+}. \quad (13)$$

In order to compare the calculated values with the experimental values and thus to provide an interpretation of the observed bands, one can first use Eq. (5) to extract the values of ε , B , and a for each of the observed bands of Sect. 3. From the value of ε one can then obtain the values of ε_K . Since we shall consider both particle (p) and hole (h) states, the relationship between ε_K and ε is

$$\begin{aligned} p &: \varepsilon_K = \varepsilon - \varepsilon_{K^P=3/2^+}, \\ h &: \varepsilon_K = -\varepsilon - \varepsilon_{K^P=3/2^+}. \end{aligned} \quad (14)$$

From the values of ε_K we can then obtain the values of ε'_K using

$$\varepsilon'_K = \varepsilon_K - S_n - \frac{3}{2} B_{K^P=3/2^+}, \quad (15)$$

where S_n is the neutron separation energy $S_n = 6761.16(4)$ keV and we have subtracted the energy of the ground state $J^P = K^P = 3/2^+$. The experimental values of the particle and hole intrinsic states $\varepsilon_K(\text{exp})$, $\varepsilon'_K(\text{exp})$ and the experimental decoupling parameters, $a(\text{exp})$ are shown in the center column of Fig. 3.

4.2. Assignments into bands

4.2.1. $K^P = 3/2^+(0)$

This band is the ground state band. It is observed up to $J^P = 15/2^+$ with inertial parameter $B = 138$ keV and intrinsic energy relative to the ground state $J^P = 3/2^+$ of $\varepsilon = -0.207$ MeV. This band has an anomaly at $J^P = 5/2^+$ since the energy of this state does not fit the rotational behavior, Eq. (5). This band with $\varepsilon'_K = -6.97$ MeV relative to the $^{20}\text{Ne}+n$ threshold can be associated with the calculated $K^P = 3/2^+$ band at $\varepsilon'_K = -7.22$ MeV.

4.2.2. $K^P = 1/2^-(2789)$

This band starts at $E_x = 2789$ keV. It is observed up to $J^P = 15/2^-$ with inertial parameter $B = 148$ keV, decoupling parameter $a = 0.54$ and intrinsic energy $\varepsilon = 2.824$ MeV. This band can be associated with the calculated $K^P = 1/2^-$ band at $\varepsilon'_K = -10.45$ MeV. The interpretation of this band as a "hole" band was suggested years ago by Howard *et al.* [30] on the basis of intensities in (d, p) and (p, d) reactions, following a previous theoretical article [31] and confirmed by further experiments [32]. The observed value of $\varepsilon'_K = -10.0$ MeV in this interpretation is in excellent agreement with the calculated value, as well as with the calculated value of the decoupling parameter $a = 0.64$. Further confirmation of this band as a "hole" band is obtained from an analysis of a similar band in ^{19}F and ^{19}Ne .

4.2.3. $K^P = 1/2^+(2794)$

This band starts at $E_x = 2794$ keV. It is observed up to $J^P = 9/2^+$ with inertial parameter $B = 214$ keV, decoupling parameter $a = 1.93$ and intrinsic energy $\varepsilon = 3.088$ MeV. This band can be associated with the calculated $K^P = 1/2^+$ band at $\varepsilon'_K = -9.84$ MeV. The interpretation of this band as a "hole" band was also suggested in [30]. The observed value $\varepsilon'_K = -10.3$ MeV is in excellent agreement with the calculated value, as it is the decoupling parameter calculated at $a = 2.16$. Further confirmation is obtained from an analysis of a similar band in ^{19}F , ^{19}Ne . The almost equal energy of the $1/2^+$ state of this band with the $1/2^-$ state of the band $K^P = 1/2^-(2789)$ suggests that these two bands form a parity doublet.

4.2.4. $K^P = 5/2^+(4526)$

This band starts at $E_x = 4526$ keV. It is observed up to $K^P = 13/2^+$ with inertial parameter $B = 128$ keV, and intrinsic energy $\varepsilon = 4.199$ MeV. This band can be associated with the calculated $K^P = 5/2^+$ "particle" band at $\varepsilon'_K = -4.37$ MeV. The observed value $\varepsilon'_K = -2.56$ MeV is however only in qualitative agreement with the calculated value. Howard *et al.* [30] also associate this band with the $K^P = 5/2^+$ "particle" band.

4.2.5. $K^P = 1/2^-(5690)$

This band poses some difficulties as the lowest member of the band has $J^P = 3/2^-$ and it has been the subject of many different interpretations. Our analysis agrees with the assignment of [30] as a "particle" intrinsic state originating from the $1f_{7/2}$ spherical state. The extracted values of $\varepsilon = 5.107$ MeV, ($\varepsilon'_K = -1.65$ MeV) and $a = -2.85$ are in agreement with the calculated values $\varepsilon'_K = -2.88$ MeV, $a = -2.60$. The large and negative value of a accounts for the inversion in the lowest member of the band. The inertial parameter of this band is $B = 174$ MeV. This interpretation is strongly supported by $^{20}\text{Ne}(d, p)$ data [30]. It is in disagreement with the interpretation of this band as the parity doubled band of the ground state.

4.2.6. $K^P = 3/2^+(5549)$

This band starts at $E_x = 5549$ keV. It is observed up to $J^P = 9/2^+$ with a small inertial parameter $B = 60$ keV and $\varepsilon = 5.459$ MeV. One possible interpretation of this band is as the single "particle" state with $K^P = 3/2^+$ calculated at $\varepsilon'_K = -0.37$ MeV. Another possible interpretation is that of a single particle state $K^P = 3/2^+$ at $\varepsilon'_K = -7.22$ MeV coupled to the vibrational $A'_1 : K^P = 0^+(6.72)$ of ^{20}Ne . The small inertial parameter $B = 60$ keV and the calculated value $\varepsilon'_K = -0.50$ MeV support this interpretation, which we tentatively adopt.

4.2.7. $K^P = 3/2^+(5826)$

The interpretation of this band poses several difficulties. If it assumed to have $K^P = 3/2^+$ this band starts at $E_x = 5826$ keV. It is observed up to $J^P = 9/2^+$ with a small inertial parameter $B = 58$ keV and $\varepsilon = 5.735$ MeV, ($\varepsilon'_K = -1.02$ MeV). Its interpretation is a single particle state with $K^P = 3/2^+$ at $\varepsilon'_K = -7.22$ MeV coupled to the vibrational state $A'_1 : K^P = 0^+(7.19)$ of ^{20}Ne . The small inertial parameter $B = 58$ keV and the calculated value $\varepsilon'_K = -0.03$ MeV support this interpretation. Also note that the difference $\Delta\varepsilon_K = -0.28$ MeV between this band and the band $K^P = 3/2^+(5549)$ is in agreement with the difference $\Delta\varepsilon_K = -0.47$ MeV in ^{20}Ne . An alternative interpretation is that, together with a state $J^P = 1/2^+$ at 5525 keV, it forms a $K^P = 1/2^+$ rotational band. This interpretation is however disfavored by the small inertial parameter and by the lack of spin assignment for the 5525 keV level.

The level scheme corresponding to these assignments is shown in Fig. 4.

4.3. Summary of assignments into bands and comparison with other assignments and models

In Table 3 we show a summary of our assignments into rotational bands and the corresponding values of the intrinsic energies ε , inertial parameters B and decoupling parameters a , together with an estimate of the error in extracting these values from experiment. We also show in this table, for comparison with the calculated values, the intrinsic energies ε_K and ε'_K and the character of the state: p=particle, h=hole, and v=vibration.

The assignments of states of bands 1, 3, 4, 6 agree with the assignments of [24]. They disagree for bands 2, 5 and 7. Band 2 is assigned in [24] as $K^P = 3/2^-$. This is in contrast with experiment for two reasons: (i) the $5/2^-$ member of the supposed $K = 1/2^-$ band is missing and (ii) most importantly the $B(E2; 3/2^- \rightarrow 1/2^-)$ is observed to be very large $15(13)$ W.u. $= 51.6(447)$ e^2fm^4 , as discussed in the following section. The assignment of band 7 to $K^P = 1/2^+$ is also in contrast with experiment. The authors of [24] have changed the parity of the state at 5690 keV from $J^P = 1/2^-$ [25] to $J^P = 1/2^+$.

In summary, there appear to be in ^{21}Ne three coexisting classes of rotational bands, classified in the cluster model as single-particle states (bands 1, 4 and 5), as single-hole states (bands 2 and 3), and as vibrational states (bands 6 and

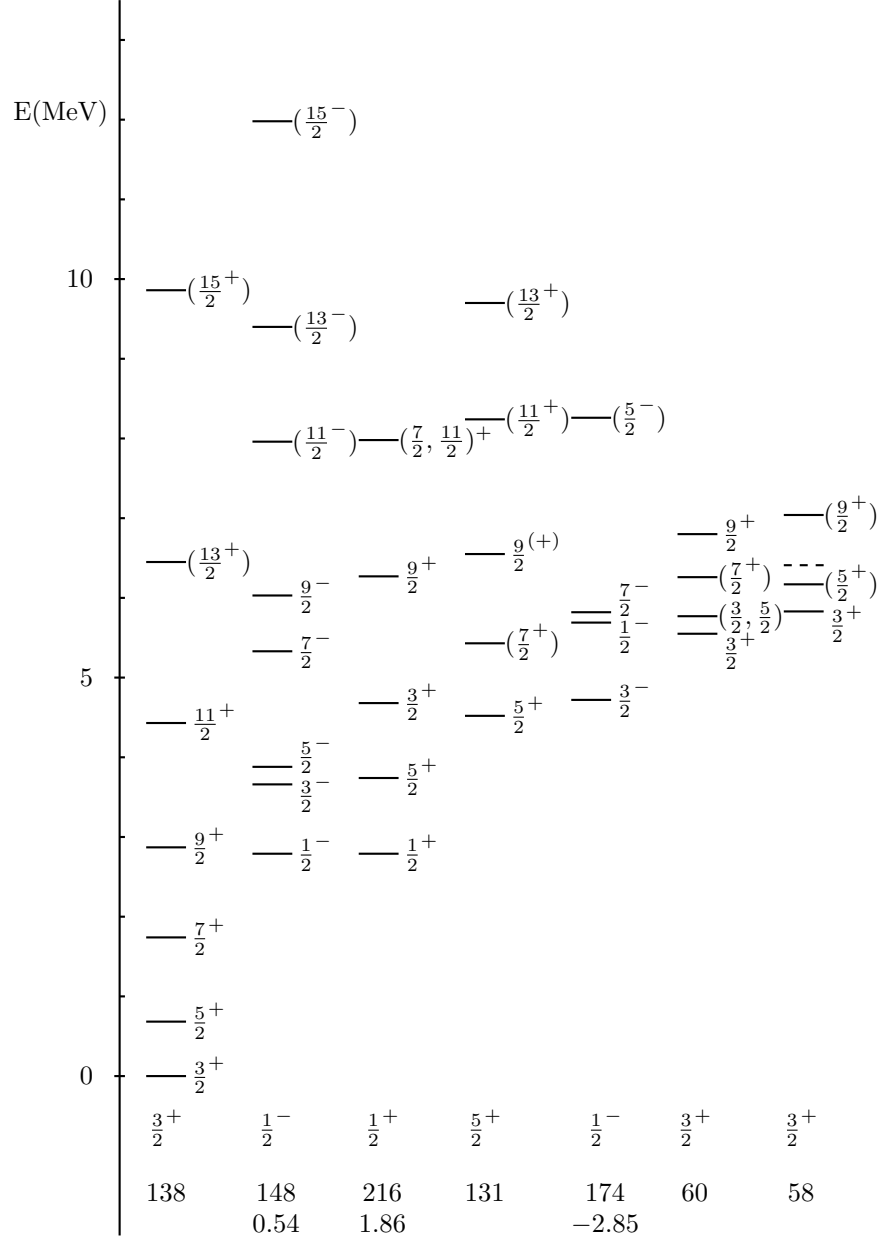


Figure 4: Cluster interpretation of the rotational bands in ^{21}Ne . The bands are labeled by K^P and the values of the rotational parameter, B , and decoupling parameter, a .

Table 3: Summary of assignments in ^{21}Ne

#	K^P	E (keV)	B (keV)	a	ε (keV)	ε_K (MeV)	ε'_K (MeV)
1 (p)	$3/2^+$	0	138(4)		-207(21)	0	-6.97
2 (h)	$1/2^-$	2789	148(12)	0.54(6)	2824(4)	-2.99	-9.96
3 (h)	$1/2^+$	2794	216(8)	1.86(4)	3088(29)	-3.31	-10.28
4 (p)	$5/2^+$	4526	131(4)		4199(32)	4.41	-2.56
5 (p)	$1/2^-$	5690	174(12)	-2.85(6)	5107(58)	5.32	-1.65
6 (v)	$3/2^+$	5549	60(2)		5459(9)	5.67	-1.30
7 (v)	$3/2^+$	5826	58(2)		5735(9)	6.17	-0.80

7). The CSM provides an excellent description of bands 1, 2 and 3, and a good description of bands 4, 5, 6 and 7. Its only drawback is the non-observation of the band $K^P = 1/2^+$ at $\varepsilon'_K = -5.44$ MeV. Although one may try to correct this problem by the introduction of *ad hoc* terms in the potential, we do not pursue this avenue further in this paper. We also note that the CSM predicts the neutron separation energy $S_n(\text{th}) = 7.01$ MeV, in very good agreement with the experimental value $S_n(\text{exp}) = 6761.14(4)$ keV.

It is of interest to compare the results of the CSM with those of the Nilsson model [29]. To this end, we show in the right column of Fig. 3 the Nilsson intrinsic energies ε_K calculated in [30]. The Nilsson model produces intrinsic energies ε_K comparable to those of the CSM and in good agreement with data. The enlarged scale of the Nilsson model relative to the CSM is due to the fact that in the Nilsson model an harmonic oscillator potential is used while in the CSM a gaussian potential is used. As in the case of CSM, the drawback of the Nilsson model is the non-observation of the band $K^P = 1/2^+$ at $\varepsilon_K = 2.82$ MeV. Also, in the Nilsson model, one cannot calculate the separation energy, S_n . The agreement between the intrinsic energies of the two models arises from the fact that the bi-pyramid can be inscribed into an ellipsoid with large deformation, as shown in Fig. 5.

Our assignments suggest the following spherical shell model interpretation: the positive parity bands 1, 3 and 4 arise mostly from $(2s1d)^5$ configurations, the negative parity band 2 arises from $(2s1d)^6(1p)^{-1}$ configuration and the negative parity band 5 from $(2s1d)^4(1f)$ configuration. Since the A'_1 vibrations in ^{20}Ne arise in the shell model from $4p-4h$ configurations, the two vibrational bands 6 and 7 in ^{21}Ne arise from configurations $(2s1d)^5 \times (4p-4h)$. Both the A'_1 bands in ^{20}Ne and $A'_1 \otimes K^P = 3/2^+$ have energies of about 6 MeV which is the energy of the expected $4p-4h$ states.

4.4. Cluster interpretation of the observed bands

The particle and vibrational bands of Table 3 can be identified as states of the cluster structure $^{20}\text{Ne}+n$. They arise from coupling of the rotational

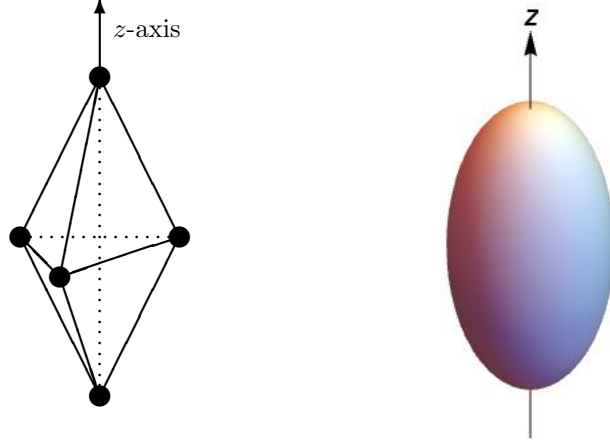


Figure 5: The bi-pyramidal structure with \mathcal{D}_{3h} symmetry and its osculating ellipsoid with $\mathcal{D}_{\infty h}$ symmetry.

bands of ^{20}Ne denoted by $\Gamma : K_c^{P_c}(E_c)$ with single-particle states denoted by $\Omega : K_p^{P_p}(E_p)$. The values of K , the total projection on the symmetry axis, and P , the total parity are given by

$$K = |K_c \pm K_p| , \quad P = P_c P_p . \quad (16)$$

(If $K_c \neq 0$, there are two values of K). The three particle bands $K^P = 3/2^+(0.0)$, $K^P = 5/2^+(4526)$, $K^P = 1/2^-(5690)$ are the corresponding particle intrinsic states coupled to the ground state of ^{20}Ne , $A'_1 : K^P = 0^+(0.0)$. The two vibrational bands $K^P = 3/2^+(5549)$ and $K^P = 3/2^+(5826)$ are the particle state $K^P = 3/2^+$ coupled to the vibrations of ^{20}Ne , $A'_1 : K^P = 0^+(6.72)$ and $A'_1 = 0^+(7.19)$. On the basis of Table 1, one would expect seven more vibrational bands. Although there is some evidence for additional bands with intrinsic energies higher than 6 MeV, the analysis of bands at these energies is made very difficult by the high density of states and we will not pursue it further in this paper. The two hole bands of Table 3, $K^P = 1/2^-(2789)$, $K^P = 1/2^+(2796)$, forming a parity doublet, can be identified as states of the cluster structure $^{19}\text{Ne}+2n$. This identification is strongly supported by the experimental spectrum of ^{19}Ne , the ground state of which is a parity doublet $K^P = 1/2^+(0.0)$, $K^P = 1/2^-(275)$. In summary, it appears that in ^{21}Ne there is the coexistence of two cluster structures, $^{20}\text{Ne}+n$ and $^{19}\text{Ne}+2n$.

5. Electromagnetic transition rates

The reduced probabilities of electromagnetic transitions in $k\alpha + x$ nuclei can be calculated using Eq. (25) of [9] as

$$\begin{aligned}
B(\lambda; \Omega', K', J'^P \rightarrow \Omega, K, J^P) &= \left| \langle J', K', \lambda, K - K' | J, K \rangle (\delta_{v,v'} G_\lambda(\Omega, \Omega') + \delta_{\Omega, \Omega'} G_{\lambda,c}) \right. \\
&\quad \left. + (-1)^{J+K} \langle J', K', \lambda, -K - K' | J, -K \rangle \right. \\
&\quad \left. \times \left(\delta_{v,v'} \tilde{G}_\lambda(\Omega, -\Omega') + \delta_{\Omega, -\Omega'} G_{\lambda,c} \right) \right|^2 \quad (17)
\end{aligned}$$

We note that the second term in Eq. (17) contributes only in the case $\lambda \geq K + K'$. Here $G_\lambda(\Omega, \Omega')$ represents the contribution of the single particle and $G_{\lambda,c}$ the contribution of the cluster. Similarly, electric and magnetic multipole moments can be calculated using Eq. (28) of [9]

$$\begin{aligned}
Q^{(\lambda)}(K, J^P) &= \sqrt{\frac{16\pi}{2\lambda+1}} \langle J, K, \lambda, 0 | J, K \rangle \langle J, J, \lambda, 0 | J, J \rangle (G_\lambda(\Omega, \Omega) + G_{\lambda,c}) , \\
\mu^{(\lambda)}(K, J^P) &= \sqrt{\frac{4\pi}{2\lambda+1}} \langle J, K, \lambda, 0 | J, K \rangle \langle J, J, \lambda, 0 | J, J \rangle (G_\lambda(\Omega, \Omega) + G_{\lambda,c}) . \quad (18)
\end{aligned}$$

Here again $G_\lambda(\Omega, \Omega)$ represents the contribution of the single particle and $G_{\lambda,c}$ of the cluster. In ^{21}Ne , the single particle is a neutron and thus it does not contribute to electric transitions, except for $E1$ transitions affected by center-of-mass corrections as given in Eq. (32) of [9]. The cluster contribution to electric transitions $E2$, $E3$, $E4$ is given by the \mathcal{D}_{3h} symmetry as in Sect. 2.2.4 of [16]. Note that the cluster calculation of electric transitions does not require the use of effective charges. Magnetic transitions are dominated by the single-particle contribution. For in-band transitions and magnetic moments, there is also a cluster contribution.

5.1. $K^P = \frac{3}{2}^+(0) \rightarrow K^P = \frac{3}{2}^+(0)$

Several transition rates have been measured for this band. The $B(E2)$ values and quadrupole moments $Q^{(2)}$ can be simply calculated as

$$\begin{aligned}
B(E2; \frac{3}{2}, J'^+ \rightarrow \frac{3}{2}, J^+) &= Q_0^2 \frac{5}{16\pi} \langle J', \frac{3}{2}, 2, 0 | J, \frac{3}{2} \rangle^2 , \\
Q^{(2)}(\frac{3}{2}, J^+) &= Q_0 \langle J, \frac{3}{2}, 2, 0 | J, \frac{3}{2} \rangle \langle J, J, 2, 0 | J, J \rangle . \quad (19)
\end{aligned}$$

The value of the intrinsic quadrupole moment in ^{21}Ne , $Q_0 = G_{2,c} \sqrt{16\pi/5}$, can be determined from the quadrupole transition $B(E2; \frac{3}{2}, \frac{5}{2}^+ \rightarrow \frac{3}{2}, \frac{3}{2}^+)$ as $Q_0(^{21}\text{Ne}) = 49.4(20) \text{ efm}^2$, in remarkable agreement with the value obtained for ^{20}Ne [16], $Q_0(^{20}\text{Ne}) = 52.5(21) \text{ efm}^2$. With the value of $Q_0 = 49.4 \text{ efm}^2$ we calculate all $B(E2)$ values and quadrupole moments as given in Tables 4 and 5.

Table 4: In-band $B(E2)$ values in e^2fm^4 and $B(M1)$ values in μ_N^2 for the $K^\pi = \frac{3}{2}^+(0)$ band. The theoretical values were obtained with $Q_0 = 49.4 \text{ efm}^2$ and $G_1(\frac{3}{2}^+) = -0.85 \mu_N$.

E_γ^{exp} (keV)	$J'^{P'}$	\rightarrow	J^P	$B(E2)$		$B(M1)$	
				Exp	Th	Exp	Th
351	$5/2^+$	\rightarrow	$3/2^+$	83.6(61)	83.2*	0.1275(25)	0.19
1394	$7/2^+$	\rightarrow	$5/2^+$	37.8(137)	52.0	0.2615(21)	0.26*
1122	$9/2^+$	\rightarrow	$7/2^+$	31.0(172)	34.0	0.43(5)	0.29
1566	$11/2^+$	\rightarrow	$9/2^+$	20.6(130)	23.8	0.36(7)	0.31
2015	$13/2^+$	\rightarrow	$11/2^+$		17.4		0.32
3409	$15/2^+$	\rightarrow	$13/2^+$		13.3		0.33
1745	$7/2^+$	\rightarrow	$3/2^+$	32.0(27)	34.7		
2516	$9/2^+$	\rightarrow	$5/2^+$	54.7(76)	52.0		
2688	$11/2^+$	\rightarrow	$7/2^+$		61.8		
3581	$13/2^+$	\rightarrow	$9/2^+$		67.9		
5424	$15/2^+$	\rightarrow	$11/2^+$		72.0		

Table 5: Spectroscopic quadrupole moment and magnetic moment of the $J^\pi = \frac{3}{2}^+$ ground state.

	Exp	Th
$Q^{(2)}(\frac{3}{2}, \frac{3}{2}^+)$	+10.3(8)	+9.9 efm^2
$\mu^{(1)}(\frac{3}{2}, \frac{3}{2}^+)$	-0.661797(5)	-0.43 μ_N

The asterisk in this and the following tables indicates that the value is used to extract the intrinsic matrix elements.

Similarly, the $B(M1)$ values and magnetic moments are given by

$$\begin{aligned}
B(M1; \frac{3}{2}, J'^+ \rightarrow \frac{3}{2}, J^+) &= \langle J', \frac{3}{2}, 1, 0 | J, \frac{3}{2} \rangle^2 \left| G_1(\frac{3}{2}^+) \right|^2, \\
\mu^{(1)}(\frac{3}{2}, J^+) &= \sqrt{\frac{4\pi}{3}} \langle J, \frac{3}{2}, 1, 0 | J, \frac{3}{2} \rangle \langle J, J, 1, 0 | J, J \rangle \\
&\quad \left[G_1(\frac{3}{2}^+) + G_{1R} \right], \tag{20}
\end{aligned}$$

where G_{1R} represents an additional contribution of the cluster. From the $B(M1; \frac{3}{2}, \frac{7}{2}^+ \rightarrow \frac{3}{2}, \frac{5}{2}^+)$ we extract the value $|G_1(\frac{3}{2}^+)| = 0.85(4) \mu_N$. From this value we can calculate all $B(M1)$ values given in Table 4. For the magnetic moment using $G_1(\frac{3}{2}^+) = -0.85 \mu_N$ and adding $G_{1R} = Z/A = 0.50 \mu_N$ we obtain the value of Table 5. The Tables 4 and 5 show that the band $K^\pi = \frac{3}{2}^+(0)$ is an almost perfect rotational band.

Table 6: In-band $B(E2)$ values in e^2fm^4 and $B(M1)$ values in μ_N^2 for the $K^P = \frac{1}{2}^-$ (2789) band. The theoretical values were obtained with $Q_0 = 49.4 \text{ efm}^2$ and $|G_1(\frac{1}{2}^-)| = 0.993 \mu_N$.

E_γ^{exp} (keV)	$J'^{P'}$	\rightarrow	J^P	$B(E2)$		$B(M1)$	
				Exp	Th	Exp	Th
874	$3/2^-$	\rightarrow	$1/2^-$	51.6(447)	48.6	0.329(43)	0.33*
221	$5/2^-$	\rightarrow	$3/2^-$		13.9		0.40
1450	$7/2^-$	\rightarrow	$5/2^-$		6.9		0.43
699	$9/2^-$	\rightarrow	$7/2^-$		4.2		0.44
1928	$11/2^-$	\rightarrow	$9/2^-$		2.8		0.45
1440	$13/2^-$	\rightarrow	$11/2^-$		2.0		0.46
2582	$15/2^-$	\rightarrow	$13/2^-$		1.5		0.46
1095	$5/2^-$	\rightarrow	$1/2^-$		48.6		
1671	$7/2^-$	\rightarrow	$3/2^-$		62.4		
2149	$9/2^-$	\rightarrow	$5/2^-$		69.4		
2627	$11/2^-$	\rightarrow	$7/2^-$		73.6		
3368	$13/2^-$	\rightarrow	$9/2^-$		76.4		
4002	$15/2^-$	\rightarrow	$11/2^-$		78.4		

5.2. $K^P = \frac{1}{2}^-$ (2789) $\rightarrow K^P = \frac{1}{2}^-$ (2789)

$B(E2)$ values and quadrupole moments for this band can be calculated with

$$\begin{aligned}
 B(E2; \tfrac{1}{2}, J'^- \rightarrow \tfrac{1}{2}, J^-) &= Q_0^2 \frac{5}{16\pi} \langle J', \tfrac{1}{2}, 2, 0 | J, \tfrac{1}{2} \rangle^2, \\
 Q^{(2)}(\tfrac{1}{2}, J^-) &= Q_0 \langle J, \tfrac{1}{2}, 2, 0 | J, \tfrac{1}{2} \rangle \langle J, J, 2, 0 | J, J \rangle. \quad (21)
 \end{aligned}$$

Although in general for $K = \frac{1}{2}$ bands both terms in Eq. (17) contribute, in this special case in which there is no single-particle contribution, only the first term remains as in Eq. (21). The results of the calculation for $B(E2)$ values are shown in Table 6, where they are compared with the only available experimental value. The large value of $B(E2; \frac{1}{2}, \frac{3}{2}^- \rightarrow \frac{1}{2}, \frac{1}{2}^-)$ is strong evidence for the assignment of this band to $K^P = \frac{1}{2}^-$, in contrast with the assignment of [24]. Similarly one can calculate $B(M1)$ values and magnetic moments for this band as

$$\begin{aligned}
 B(M1; \tfrac{1}{2}, J'^- \rightarrow \tfrac{1}{2}, J^-) &= \langle J', \tfrac{1}{2}, 1, 0 | J, \tfrac{1}{2} \rangle^2 \left| G_1(\tfrac{1}{2}^-) \right|^2, \\
 \mu^{(1)}(\tfrac{1}{2}, J^-) &= \sqrt{\frac{4\pi}{3}} \langle J, \tfrac{1}{2}, 1, 0 | J, \tfrac{1}{2} \rangle \langle J, J, 1, 0 | J, J \rangle \\
 &\quad \left[G_1(\tfrac{1}{2}^-) + G_{1R} \right]. \quad (22)
 \end{aligned}$$

We remark that the measured value of the $B(E2; \frac{1}{2}, \frac{3}{2}^- \rightarrow \frac{1}{2}, \frac{1}{2}^-)$ is strong evidence for the cluster structure of ^{21}Ne as $^{20}\text{Ne}+n$ because it agrees within

experimental error with the calculated value with $Q_0 = 49.4 \text{ efm}^2$, which in turn agrees with Q_0 in ^{20}Ne . No new parameter is involved in the calculation of the quadrupole transitions. The value of $|G_1(\frac{1}{2}^-)|$ is determined from the measured value of $B(M1; \frac{1}{2}, \frac{3}{2}^- \rightarrow \frac{1}{2}, \frac{1}{2}^-)$ to be $0.993 \mu_N$. The $B(M1)$ values are given in Table 6.

5.3. $K^P = \frac{1}{2}^- (2789) \rightarrow K^P = \frac{3}{2}^+ (0)$

Several out of band $E1$ transitions rates from $K^P = \frac{1}{2}^- (2789)$ to the ground state band $K^P = \frac{3}{2}^+ (0)$ have been measured [25]. $E1$ transition rates are difficult to calculate because they vanish in $N = Z$ nuclei due to isospin considerations. In ^{21}Ne , they arise from center-of-mass corrections [9]. Within the cluster model, they can be parametrized in terms of an effective dipole moment Q_{1m} ($m = 0, \pm 1$). For the $\Delta K = 1$ transitions considered here, they can be calculated using

$$B(E1; \frac{1}{2}, J'^- \rightarrow \frac{3}{2}, J^+) = 2(Q_{11})^2 \frac{3}{4\pi} \langle J', \frac{1}{2}, 1, 1 | J, \frac{3}{2} \rangle^2, \quad (23)$$

the factor of 2 arising from the sum over $Q_{1,+1}$ and $Q_{1,-1}$. By fitting the value of the dipole moment Q_{11} to the dipole transition $B(E1; \frac{1}{2}, \frac{5}{2}^- \rightarrow \frac{3}{2}, \frac{5}{2}^+)$ we obtain $Q_{11} = 3.45 \times 10^{-2} \text{ efm}$. Table 7 shows that the calculated values are in excellent agreement with experiment.

The extraction of the electric dipole moment in cluster models has been the subject of a recent investigation [24]. The dipole moment D of [24] is related to Q_{11} by

$$2(Q_{11})^2 = (D)^2. \quad (24)$$

We obtain from $Q_{11} = 3.45 \times 10^{-2} \text{ efm}$, $D = 0.0488(26) \text{ efm}$. Wheldon *et al.* extract the dipole moment assuming that the $J^P = \frac{9}{2}^-$ state is part of a $K^P = \frac{3}{2}^-$ band obtaining $D = 0.0337(79) \text{ efm}$ (from the transition $\frac{9}{2}^- \rightarrow \frac{7}{2}^+$) and $D = 0.097(19) \text{ efm}$ (from $\frac{9}{2}^- \rightarrow \frac{9}{2}^+$) [24]. These values agree only at the 3σ level. If we extract the dipole moment assuming the $J^P = \frac{9}{2}^-$ state to be part of a $K^P = \frac{1}{2}^-$ band we obtain $D = 0.0450(27)$ (from $\frac{9}{2}^- \rightarrow \frac{9}{2}^+$) and $D = 0.0596(77) \text{ efm}$ (from $\frac{9}{2}^- \rightarrow \frac{7}{2}^+$). These values are within experimental error thus confirming our assignment.

\mathcal{D}_{3h} symmetry implies large $E2$, $E3$ and $E4$ transition rates [5]. In [16] $E3$ transitions in ^{20}Ne have been analyzed. The two observed $\Delta K = 2$ transitions have been analyzed by using

$$B(E3; \frac{1}{2}, J'^- \rightarrow \frac{3}{2}, J^+) = 2(Q_{32})^2 \langle J', -\frac{1}{2}, 3, 2 | J, \frac{3}{2} \rangle^2, \quad (25)$$

where Q_{32} is the octupole moment. The $B(E3)$ value in Table 7 was obtained by using the same value for the octupole moment as in the analysis of $E3$ transitions in ^{20}Ne , $Q_{32} = 16.3 \text{ efm}^3$ [16]. The large experimental value of the octupole transition $B(E3; \frac{1}{2}, \frac{1}{2}^- \rightarrow \frac{3}{2}, \frac{5}{2}^+) = 13(7) \text{ W.u.} = 340(183) \text{ e}^2\text{fm}^6$ is further evidence of the cluster structure of ^{21}Ne .

Table 7: $K^P = \frac{1}{2}^- (2789)$ to $K^P = \frac{3}{2}^+ (0)$ interband $10^4 \times B(E1)$ values in e^2fm^2 and $B(E3)$ values in e^2fm^6 . The theoretical values were obtained with $Q_{11} = 3.45 \times 10^{-2} \text{ efm}$ and $Q_{32} = 16.3 \text{ efm}^3$.

E_γ^{exp} (keV)	$J'^{P'}$	\rightarrow	J^P	$B(E1)$	
				Exp	Th
2789	$1/2^-$	\rightarrow	$3/2^+$		5.69
3312	$3/2^-$	\rightarrow	$5/2^+$	1.09(12)	3.41
3663	$3/2^-$	\rightarrow	$3/2^+$		2.28
2139	$5/2^-$	\rightarrow	$7/2^+$		2.71
3533	$5/2^-$	\rightarrow	$5/2^+$	2.6(3)	2.60*
3884	$5/2^-$	\rightarrow	$3/2^+$	0.65(11)	0.38
2467	$7/2^-$	\rightarrow	$9/2^+$		2.37
3589	$7/2^-$	\rightarrow	$7/2^+$		2.71
4983	$7/2^-$	\rightarrow	$5/2^+$		0.61
1600	$9/2^-$	\rightarrow	$11/2^+$		2.17
3166	$9/2^-$	\rightarrow	$9/2^+$	2.35(29)	2.76
4288	$9/2^-$	\rightarrow	$7/2^+$	1.13(29)	0.76
1513	$11/2^-$	\rightarrow	$13/2^+$		2.04
3528	$11/2^-$	\rightarrow	$11/2^+$		2.78
5094	$11/2^-$	\rightarrow	$9/2^+$		0.86
(-456)	$13/2^-$	\rightarrow	$15/2^+$		1.95
2953	$13/2^-$	\rightarrow	$13/2^+$		2.80
4968	$13/2^-$	\rightarrow	$11/2^+$		0.94

E_γ^{exp} (keV)	$J'^{P'}$	\rightarrow	J^P	$B(E3)$	
				Exp	Th
2438	$1/2^-$	\rightarrow	$5/2^+$	340(183)	380

5.4. $K^P = \frac{1}{2}^- (5690) \rightarrow K^P = \frac{1}{2}^- (5690)$

No transition rates have been measured for this band. However, the observed transition between the $J^P = \frac{1}{2}^-$ and $\frac{3}{2}^-$ members of this band strongly support our interpretation of this band as $K^P = \frac{1}{2}^-$. The calculated values with $Q_0 = 49.4 \text{ efm}^2$ and with the estimated value $|G_1(\frac{1}{2}^-)| = 1.0 \mu_N$ are given in Table 8.

5.5. $K^P = \frac{1}{2}^+ (2794) \rightarrow K^P = \frac{1}{2}^+ (2794)$ and $K^P = \frac{1}{2}^+ (2794) \rightarrow K^P = \frac{3}{2}^+ (0)$

In band $B(E2)$ values and quadrupole moments are calculated using Eq. (21). The same comments apply here as in the paragraph after these equations. $B(M1)$ values and magnetic moments are calculated with Eq. (22). The results are given in Table 9. Only one $B(M1)$ value and no $B(E2)$ values are available. Therefore no direct test of the cluster calculation can be made.

Table 8: In-band $B(E2)$ values in e^2fm^4 and $B(M1)$ values in μ_N^2 for the $K^P = \frac{3}{2}^-$ (4725) band. The theoretical values were obtained with $Q_0 = 49.4 \text{ efm}^2$ and $|G_1(\frac{1}{2}^-)| = 1.0 \mu_N$. E_γ^{exp} values are not given here because of the uncertainty in the assignment of states.

$J'P'$	\rightarrow	J^P	$B(E2)$		$B(M1)$	
			Exp	Th	Exp	Th
$3/2^-$	\rightarrow	$1/2^-$		48.6		0.33
$5/2^-$	\rightarrow	$3/2^-$		13.9		0.40
$7/2^-$	\rightarrow	$5/2^-$		6.9		0.43
$9/2^-$	\rightarrow	$7/2^-$		4.2		0.44
$5/2^-$	\rightarrow	$1/2^-$		48.6		
$7/2^-$	\rightarrow	$3/2^-$		62.4		
$9/2^-$	\rightarrow	$5/2^-$		69.4		

Table 9: In-band $B(E2)$ values in e^2fm^4 and $B(M1)$ values in μ_N^2 for the $K^P = \frac{1}{2}^+$ (2794) band. The theoretical values were obtained with $Q_0 = 49.4 \text{ efm}^2$ and $|G_1(\frac{1}{2}^+)| = 0.193 \mu_N$.

E_γ^{exp} (keV)	$J'P'$	\rightarrow	J^P	$B(E2)$		$B(M1)$	
				Exp	Th	Exp	Th
1890	$3/2^+$	\rightarrow	$1/2^+$		48.6	0.0124(39)	0.013*
(-948)	$5/2^+$	\rightarrow	$3/2^+$		13.9		0.015
4246	$7/2^+$	\rightarrow	$5/2^+$		6.9		0.016
(-1715)	$9/2^+$	\rightarrow	$7/2^+$		4.2		0.017
	$11/2^+$	\rightarrow	$9/2^+$		2.8		0.018
942	$5/2^+$	\rightarrow	$1/2^+$		48.6		
3298	$7/2^+$	\rightarrow	$3/2^+$		62.4		
2531	$9/2^+$	\rightarrow	$5/2^+$		69.4		
	$11/2^+$	\rightarrow	$7/2^+$		73.6		

$M1$ transitions from the band $K^P = \frac{1}{2}^+$ (2794) to the ground state band $K^P = \frac{3}{2}^+$ (0) can be calculated by

$$B(M1; \frac{1}{2}, J'^+ \rightarrow \frac{3}{2}, J^+) = \langle J', \frac{1}{2}, 1, 1 | J, \frac{3}{2} \rangle^2 \left| G_1(\frac{1}{2}^+, \frac{3}{2}^+) \right|^2. \quad (26)$$

The value of $G_1(\frac{1}{2}^+, \frac{3}{2}^+)$ can be fitted to the transition $B(M1; \frac{1}{2}, \frac{3}{2}^+ \rightarrow \frac{3}{2}, \frac{3}{2}^+)$ to give $|G_1(\frac{1}{2}^+, \frac{3}{2}^+)| = 0.180 \mu_N$. $E2$ transitions to the ground state vanish in the cluster model since it is a neutron transition between two different intrinsic states. The results are given in Table 10.

Table 10: $K^P = \frac{1}{2}^+(2794)$ to $K^P = \frac{3}{2}^+(0)$ interband $B(E2)$ values in e^2fm^4 and $B(M1)$ values in μ_N^2 . The theoretical values were obtained with $Q_0 = 49.4 \text{ efm}^2$ and $|G_1(\frac{1}{2}^+, \frac{3}{2}^+)| = 0.180 \mu_N$.

E_γ^{exp} (keV)	$J'^{P'}$	\rightarrow	J^P	$B(E2)$		$B(M1)$	
				Exp	Th	Exp	Th
2794	$1/2^+$	\rightarrow	$3/2^+$	0		0.329(43)	0.032
4684	$3/2^+$	\rightarrow	$3/2^+$	0		0.0127(36)	0.013*
4333	$3/2^+$	\rightarrow	$5/2^+$	0		0.027(9)	0.019

Table 11: In-band $B(E2)$ values in e^2fm^4 and $B(M1)$ values in μ_N^2 for the $K^P = \frac{5}{2}^+(4525)$ band. The theoretical values were obtained with $Q_0 = 49.4 \text{ efm}^2$ and $|G_1(5/2^+)| = 1.45 \mu_N$.

E_γ^{exp} (keV)	$J'^{P'}$	\rightarrow	J^P	$B(E2)$		$B(M1)$	
				Exp	Th	Exp	Th
905	$7/2^+$	\rightarrow	$5/2^+$		86.7		0.45*
1123	$9/2^+$	\rightarrow	$7/2^+$		73.6		0.65
1686	$11/2^+$	\rightarrow	$9/2^+$		56.6		0.76
2028	$9/2^+$	\rightarrow	$5/2^+$		24.3		
2809	$11/2^+$	\rightarrow	$7/2^+$		41.2		

5.6. $K^P = \frac{5}{2}^+(4526) \rightarrow K^P = \frac{5}{2}^+(4526)$

$B(E2)$ and $B(M1)$ values for this band can be calculated using

$$\begin{aligned}
B(E2; \frac{5}{2}, J'^+ \rightarrow \frac{5}{2}, J^+) &= Q_0^2 \frac{5}{16\pi} \langle J', \frac{5}{2}, 2, 0 | J, \frac{5}{2} \rangle^2 \\
B(M1; \frac{5}{2}, J'^+ \rightarrow \frac{5}{2}, J^+) &= \langle J', \frac{5}{2}, 1, 0 | J, \frac{5}{2} \rangle^2 \left| G_1(\frac{5}{2}^+) \right|^2. \quad (27)
\end{aligned}$$

Results are given in Table 11. No experimental data are available. $B(M1)$ values are calculated using an estimated value of $|G_1(\frac{5}{2}^+)| = 1.45 \mu_N$.

5.7. $K^P = \frac{3}{2}^+(5549) \rightarrow K^P = \frac{3}{2}^+(5549)$ and $K^P = \frac{3}{2}^+(5826) \rightarrow K^P = \frac{3}{2}^+(5826)$

$B(E2)$ and $B(M1)$ values can be calculated using Eqs. (19) and (20). The calculated values obtained with $Q_0 = 49.4 \text{ efm}^2$ and $|G_1(\frac{3}{2}^+)| = 0.85 \mu_N$, i.e. the same values as for the ground state band, are given in Table 12. No data are available for these bands.

These bands are expected to decay to the ground state band in the same way as the corresponding bands in ^{20}Ne , $K^P = 0^+(6.72)$ and $K^P = 0^+(7.19)$, decay

Table 12: In-band $B(E2)$ values in e^2fm^4 and $B(M1)$ values in μ_N^2 for the $K^P = \frac{3}{2}^+(5549)/K^P = \frac{3}{2}^+(5826)$ bands. The theoretical values were obtained with $Q_0 = 49.4 \text{ efm}^2$ and $|G_1(3/2^+)| = 0.85 \mu_N$.

E_γ^{exp} (keV)	$J^{P'}$	\rightarrow	J^P	$B(E2)$		$B(M1)$	
				Exp	Th	Exp	Th
224/ 348	$5/2^+$	\rightarrow	$3/2^+$		83.2		0.19
490/(238)	$7/2^+$	\rightarrow	$5/2^+$		52.0		0.26
535/(630)	$9/2^+$	\rightarrow	$7/2^+$		34.0		0.29

Table 13: $K^P = \frac{3}{2}^+(5549)/K^P = \frac{3}{2}^+(5826)$ to $K^P = \frac{3}{2}^+(0)$ interband $B(E2)$ values in e^2fm^4 . The theoretical values were obtained with $Q_{0t} = 2.20 \text{ efm}^2$.

E_γ^{exp} (keV)	$J^{P'}$	\rightarrow	J^P	Th	$K^P = \frac{3}{2}^+$ (5549)	$K^P = \frac{3}{2}^+$ (5826)
5549/5826	$3/2^+$	\rightarrow	$3/2^+$	0.097	0.055(24)	
5198/5475	$3/2^+$	\rightarrow	$5/2^+$	0.248		
3804/4081	$3/2^+$	\rightarrow	$7/2^+$	0.138		
5773/6174	$5/2^+$	\rightarrow	$3/2^+$	0.166		
5422/5823	$5/2^+$	\rightarrow	$5/2^+$	0.007		
4028/4429	$5/2^+$	\rightarrow	$7/2^+$	0.138*		0.138(172)
2906/3307	$5/2^+$	\rightarrow	$9/2^+$	0.172		

to the ground state band $K^P = 0^+(0)$. The transition moment for these decays in ^{20}Ne is [7] $Q_{0t} = 10.7 \text{ efm}^2$. Out of band transitions $K^P = \frac{3}{2}^+(5549/5826) \rightarrow K^P = \frac{3}{2}^+(0)$ can be calculated using

$$B(E2; \frac{3}{2}, J'^+ \rightarrow \frac{3}{2}, J^+) = (Q_{0t})^2 \frac{5}{16\pi} \langle J', \frac{3}{2}, 2, 0 | J, \frac{3}{2} \rangle^2, \quad (28)$$

The value of the transition moment, Q_{0t} , is determined from the transition $B(E2; \frac{3}{2}, \frac{5}{2}^+ \rightarrow \frac{3}{2}, \frac{7}{2}^+)$ from the band $K^P = \frac{3}{2}^+(5826)$ to the ground state band to be 2.20 efm^2 . The calculated values for some decays of the two bands $K^P = \frac{3}{2}^+(5549)$ and $K^P = \frac{3}{2}^+(5826)$ to the ground state band are shown in Table 13. The same transition moment Q_{0t} appears to describe the decay of both bands.

6. Structure of ^{21}Na

We assume for ^{21}Na a structure similar to ^{21}Ne , with the odd neutron replaced by an odd-proton, and perform an analysis of experimental data [25] similar to that of Sect. 3.

Table 14: Rotational bands in ^{21}Na

$K^P(E_{\text{exc}})$	J^P	E_{exp}	E_{th}
$3/2^+(0)$	$3/2^+$	0	0
	$5/2^+$	332	685
	$7/2^+$	1716	1644
	$9/2^+$	2829	2877
	$11/2^+$	(4419)	4380
$1/2^-(2798)$	$1/2^-$	2798	2798
	$3/2^-$	3679	3679
	$5/2^-$	3862	3861
	$7/2^-$	5815	5916
$1/2^+(2424)$	$1/2^+$	2424	2424
	$3/2^+$	4468	4461
	$5/2^+$	3544	3544
$5/2^+(4294)$	$5/2^+$	4294	4294
	$7/2^+$	(5380)	5379
$1/2^-(4984)$	$1/2^-$	4984	
	$3/2^-$	4170	
$1/2^+(5457)$	$1/2^+$	5457	

6.1. Assignments of states to bands

We are able to identify in this case four rotational bands for which the values of ε, B and a can be extracted, and fragments of two more bands as shown in Table 14 and Fig. 6.

6.2. Cluster interpretation of rotational bands

The four observed rotational bands in ^{21}Na are the mirror bands of the four rotational bands $K^P = 3/2^+(0)$, $1/2^-(2789)$, $1/2^+(2794)$ and $5/2^+(4526)$ in ^{21}Ne . The fifth band is the mirror of the $K^P = 1/2^-(5690)$ band in ^{21}Ne . The sixth band does not have a direct counterpart in ^{21}Ne . It is shown here because it may be evidence for the missing $K^P = 1/2^+$ particle band in ^{21}Ne with a tentative state at 5525 keV. In order to analyze the band structure in ^{21}Na we use the CSM Hamiltonian of Eq. (7), to which the Coulomb interaction of the odd-proton with ^{20}Ne is added

$$H = \frac{\vec{p}^2}{2m} + V(\vec{r}) + V_{so}(\vec{r}) + V_C(\vec{r}). \quad (29)$$

The expression for the Coulomb interaction was given in Eq. (32) of [21]. For simplicity in the numerical solution of the eigenvalue problem, we approximate $V_C(\vec{r})$ with a form similar to $V(\vec{r})$ of Eq. (8), but different values of V_1, V_2 and α_1, α_2 , namely $V_{1C} = V_{2C} = 1.71 \text{ MeV}$ and $\alpha_{1C} = \alpha_{2C} = 0.034 \text{ fm}^{-2}$. The

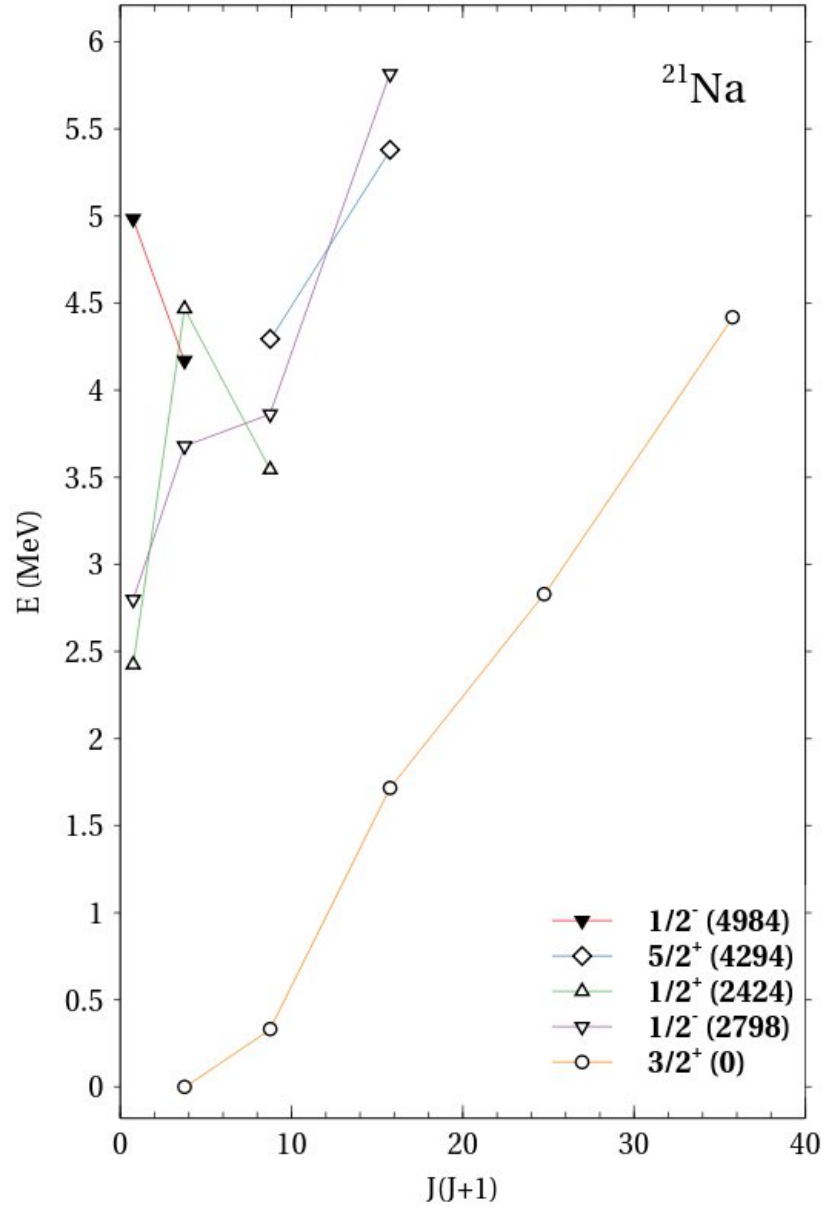


Figure 6: Energies of assigned states in ^{21}Na to rotational bands as a function of $J(J+1)$.

Table 15: Summary of assignments in ^{21}Na

#	K^P	$E(\text{keV})$	$B(\text{keV})$	a	$\varepsilon(\text{keV})$	$\varepsilon_K(\text{MeV})$	$\varepsilon'_K(\text{MeV})$
1 (p)	$3/2^+$	0	137(4)		-206(21)	0	-2.63
2 (h)	$1/2^-$	2798	165(12)	0.78(6)	2845(5)	-3.05	-5.68
3 (h)	$1/2^+$	2424	248(16)	1.74(8)	2731(30)	-2.94	-5.57
4 (p)	$5/2^+$	4294	155(12)		3907(39)	4.11	1.48

Table 16: Coulomb displacement energies for ^{21}Ne – ^{21}Na . All values in MeV.

#	K^P	$\varepsilon'_K(\text{th})$ ^{21}Ne ^{21}Na		$\Delta\varepsilon'_K(\text{th})$	$\varepsilon'_K(\text{exp})$ ^{21}Ne ^{21}Na		$\Delta\varepsilon'_K(\text{exp})$
1 (p)	$3/2^+$	-7.22	-2.96	4.26	-6.97	-2.63	4.34(2)
2 (h)	$1/2^-$	-10.45	-5.54	4.91	-9.96	-5.68	4.28(4)
3 (h)	$1/2^+$	-9.84	-5.48	4.36	-10.28	-5.57	4.71(4)
4 (p)	$5/2^+$	-4.37	-0.16	4.21	-2.56	1.48	4.04(2)

single-particle intrinsic levels with the Coulomb interaction included are given in the left side of Fig. 7.

We calculate the proton separation energy $S_p(\text{calc}) = 2.75$ MeV to be compared with the experimental value $S_p(\text{exp}) = 2.42168(28)$ MeV. This is a remarkable result since there are no parameters in the calculation, the strength of the Coulomb interaction being fixed by the charge of ^{20}Ne , $Z = 10$. Using Eq. (5) we can extract the values of ε , B and a for each of the four observed bands, a summary of which is given in Table 15. In Fig. 8 we show the corresponding level scheme.

The cluster interpretation of the four observed bands in ^{21}Na is similar to that of their mirror bands in ^{21}Ne and we do not repeat it here. We consider instead the Coulomb displacement energies ΔE_K of the four observed bands in ^{21}Na . In Table 16 we compare the calculated values with the experimental values.

While the CSM correctly describes the Coulomb displacement energies of the particle states $K^P = 3/2^+$ and $5/2^+$, it fails in describing the displacement energies of the hole states $K^P = 1/2^-$ and $1/2^+$. This failure may be due to the neglect of residual interactions in the single particle approach of this paper. While the particle states in ^{21}Na can be associated with the cluster structure $^{20}\text{Ne}+p$, the hole states are associated with the $^{19}\text{F}+2p$ cluster structure. The latter structure has an additional proton-proton interaction not included in the CSM.

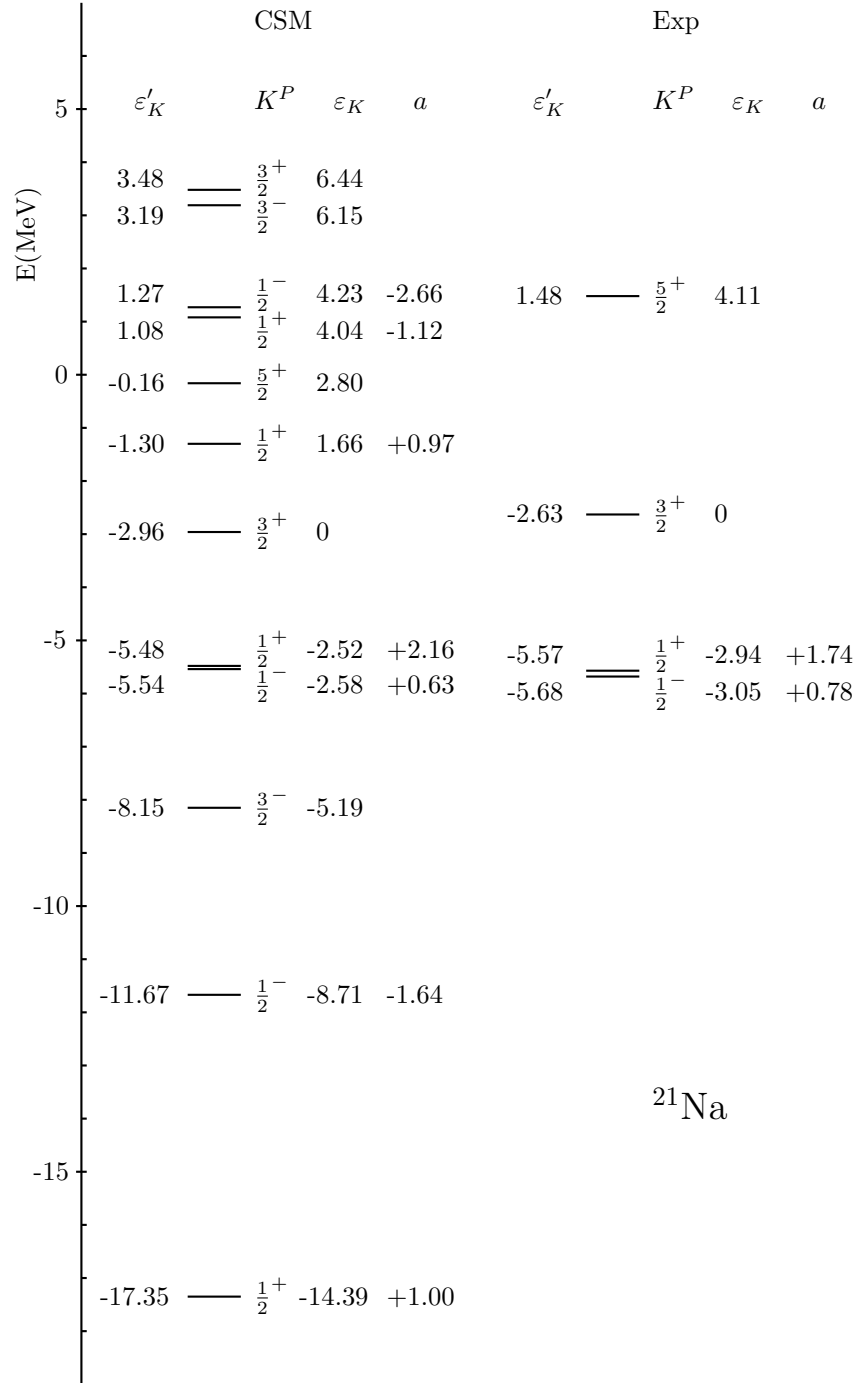


Figure 7: Energies of the intrinsic proton states in ^{21}Na in the CSM (left) compared with the experimental intrinsic energies (right).

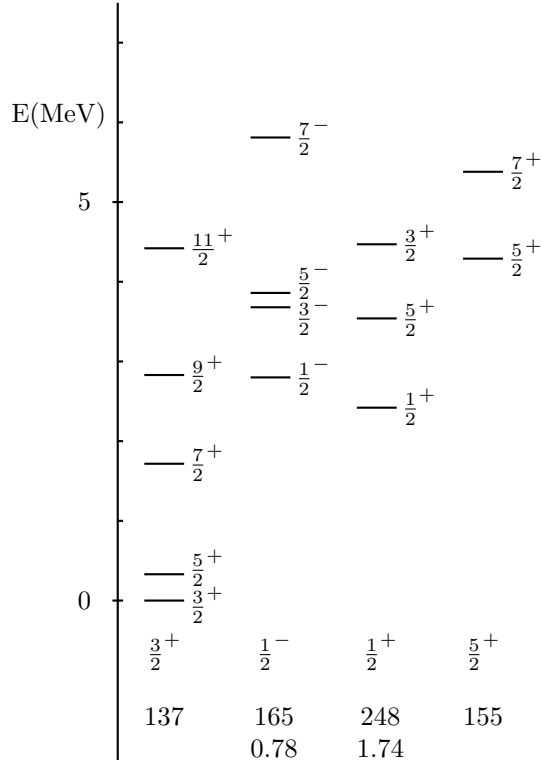


Figure 8: Cluster interpretation of the rotational bands in ^{21}Na . The bands are labeled by K^P and the values of the rotational parameter, B , and decoupling parameter, a .

6.3. Electromagnetic transition rates

The available experimental information in ^{21}Na is not as extensive as in ^{21}Ne . $B(\lambda)$ values and electric and magnetic moments can be calculated still as in Eqs. (17-18). However, in ^{21}Na the single particle is a proton and thus there is a contribution to electric transitions.

6.3.1. $K^P = \frac{3}{2}^+(0) \rightarrow K^P = \frac{3}{2}^+(0)$

Some transition rates have been measured for this band. The $B(E2)$ values and quadrupole moments $Q^{(2)}$ can be calculated as in Eq. (19) but with $Q_0 = Q_{0c} + Q_{0p}$. From the $B(E2; \frac{3}{2}, \frac{5}{2}^+ \rightarrow \frac{3}{2}, \frac{3}{2}^+)$ we extract the value of Q_0 in ^{21}Na to be $Q_0(^{21}\text{Na}) = 62.7(20) \text{ efm}^2$. Using the value of $Q_{0c}(^{21}\text{Ne}) = 49.4(20) \text{ efm}^2$, we obtain $Q_{0p} = 13.3(20) \text{ efm}^2$. With the value of $Q_0 = 62.7 \text{ efm}^2$ we calculate all $B(E2)$ values and quadrupole moments as given in Tables 17 and 18.

Similarly, the $B(M1)$ values and magnetic moments are given by Eq. (20). From the $B(M1; \frac{3}{2}, \frac{7}{2}^+ \rightarrow \frac{3}{2}, \frac{5}{2}^+)$ we extract the value $|G_1(3/2^+)| = 1.0(3) \mu_N$. With this value we calculate the $B(M1)$ values given in Table 17. Using $G_1(3/2^+) = 1.0 \mu_N$ and adding $G_{1R} = 0.50 \mu_N$ we obtain the magnetic

Table 17: In-band $B(E2)$ values in e^2fm^4 and $B(M1)$ values in μ_N^2 for the $K^P = \frac{3}{2}^+(0)$ band. The theoretical values were obtained with $Q_0 = 62.7 \text{ efm}^2$ and $|G_1(\frac{3}{2}^+)| = 1.0 \mu_N$.

E_γ^{exp} (keV)	$J'^{P'}$	\rightarrow	J^P	$B(E2)$		$B(M1)$	
				Exp	Th	Exp	Th
332	$5/2^+$	\rightarrow	$3/2^+$	134.2(103)	134.0*	0.151(2)	0.27
1384	$7/2^+$	\rightarrow	$5/2^+$	55.0(270)	83.7	0.358(89)	0.36*
1716	$7/2^+$	\rightarrow	$3/2^+$	72.3(275)	55.9		

Table 18: Spectroscopic quadrupole moment in efm^2 and magnetic moment in μ_N of the $J^P = \frac{3}{2}^+$ ground state.

	Exp	Th
$Q^{(2)}(\frac{3}{2}, \frac{3}{2}^+)$	+12.4(14)	+12.6 efm^2
$\mu^{(1)}(\frac{3}{2}, \frac{3}{2}^+)$	+2.38630(10)	+1.84 μ_N

moment given in Table 18. While the electric transitions and quadruple moment appear to be well described by the cluster model, the magnetic moment is underestimated by 20 %.

7. Summary and conclusions

In this article, we have investigated the structure of ^{21}Ne and its mirror nucleus ^{21}Na , and analyzed it in terms of the cluster shell model (CSM) [21]. The structure of these nuclei appears to be rather complex with three types of rotational bands, particle bands, hole bands and vibrational bands. In ^{21}Ne , three particle bands, $K^P = 3/2^+(0)$, $5/2^+(4526)$ and $1/2^-(5690)$, two hole bands, $K^P = 1/2^-(2789)$ and $1/2^+(2794)$, and two vibrational bands, $K^P = 3/2^+(5549)$ and $3/2^+(5826)$ have been identified, while in ^{21}Na only two particle bands, $K^P = 3/2^+(0.0)$ and $5/2^+(4294)$, and two hole bands, $K^P = 1/2^-(2798)$ and $1/2^+(2424)$ have been clearly identified, together with some fragments of two bands with $K^P = 1/2^-(4984)$ and $1/2^+(5457)$. The CSM appears to describe most of the observed properties of these bands well, with the exception of the non-occurrence of a low-lying $K^P = 1/2^+$ particle band in addition to the observed $K^P = 1/2^+(2794)$ hole band and of the Coulomb displacement energy of the hole bands. The observed properties of the rotational bands in ^{21}Ne and ^{21}Na support the cluster interpretation of the particle bands as $^{20}\text{Ne}+n$ and $^{20}\text{Ne}+p$ and of the hole bands as $^{19}\text{Ne}+2n$ and $^{19}\text{F}+2p$.

States in a bi-pyramidal potential have features similar to those of states in an ellipsoidal potential (Nilsson model). This is due to the fact that the bi-

pyramid can be inscribed into an ellipsoid. The Nilsson model gives therefore a description of the observed single particle states in ^{21}Ne as good as the cluster model. As discussed in [16] the main difference between the cluster [1] and the quadrupole collective [33] description of ^{20}Ne is in the corresponding vibrational spectra. For a bi-pyramid one has 9 vibrations, 3 singly degenerate and 3 doubly degenerate, while for the ellipsoid one has three vibrations, one singly degenerate (β -vibration) and one doubly degenerate (γ -vibration). In ^{21}Ne one therefore expects a difference between vibrational states for the cluster and the Nilsson model. Two of these vibrational states have been clearly identified, $K^P = 3/2^+(5549)$ and $3/2^+(5826)$, pointing out to the cluster interpretation, since in the Nilsson interpretation one expects only one band with $K^P = 3/2^+$ (β -vibration). Additional vibrational bands appear to be present at higher excitation energy ≥ 6 MeV with $K^P = 1/2^-$ and $3/2^-$, but their identification is very difficult due to the high density of states at this excitation energy.

Our assignment of states into bands has relied mainly on energies and electromagnetic transition rates. Our identification as particle or hole states has relied on intensities of $^{20}\text{Ne}(d,p)^{21}\text{Ne}$ (for particle states) and $^{22}\text{Ne}(p,d)^{21}\text{Ne}$ reactions (for hole states) [30]. Our assignments agree only in part with those of [24]. These authors use the incomplete fusion reaction $^{16}\text{O}(^7\text{Li},pn)^{21}\text{Ne}$ to study states in ^{21}Ne . It appears that this reaction populate strongly the ground state band $K^P = 3/2^+$ and the two hole bands, $K^P = 1/2^-$ and $1/2^+$, and weakly the states $J^P = 3/2^-$ at 4723 keV, $9/2^{(-)}$ at 6642 keV and $(7/2^-)$ at 7370 keV. In the incomplete fusion reaction, 2 protons and 3 neutrons are transferred. If we decompose this transfer into $^4\text{He}+n$ and $^3\text{He}+2n$ we can reconcile the fusion reaction results with our and Nilsson assignments into particle states and hole states.

Finally, the analysis of the rotational bands of ^{21}Ne , ^{21}Na presented here can also provide the ground for testing microscopic theories of light nuclei, such as the SDPF interaction model of [26], in particular the extent to which cluster features can be obtained from large scale shell model calculations. In this context, also of importance it would be a large scale shell model calculation of ^{21}Na to see the extent to which the microscopic shell model can describe Coulomb displacement energies.

8. Acknowledgements

This work was supported in part under research grant IN101320 from PAPIIT-DGAPA. We wish to thank D. Mengoni for stimulating the study of ^{21}Ne following an experiment performed at LNL in Legnaro, Italy, and L. Fortunato and E. Buonocore for correspondence in the early stages of this investigation.

References

- [1] D.M. Brink, Proc. Int. School of Physics "Enrico Fermi", Course XXXVI (Academic Press, 1966).

- [2] D.M. Brink, H. Friedrich, A. Weiguny and C.W. Wong, Phys. Lett. B **33** (1970) 143.
- [3] H. Friedrich and A. Weiguny, Phys. Lett. B **35** (1971) 105.
- [4] H. Friedrich, H. Husken and A. Weiguny, Phys. Lett. B **38** (1972) 199.
- [5] R. Bijker and F. Iachello, Phys. Rev. C **61** (2000) 067305.
- [6] R. Bijker and F. Iachello, Ann. Phys. (N.Y.) **298** (2002) 334.
- [7] R. Bijker and F. Iachello, Phys. Rev. Lett. **112** (2014) 152501.
- [8] R. Bijker and F. Iachello, Nucl. Phys. A **957** (2017) 154.
- [9] V. Della Rocca and F. Iachello, Nucl. Phys. A **973** (2018) 1.
- [10] M. Freer and H.O.U. Fynbo, Prog. Part. Nucl. Phys. **78** (2014) 1.
- [11] M. Freer, et al., Phys. Rev. C **76** (2007) 034320.
- [12] O.S. Kirsebom et al., Phys. Rev. C **81** (2010) 064313.
- [13] D. Marín-Lámbarri, R. Bijker, M. Freer, M. Gai, Tz. Kokalova, D.J. Parker and C. Wheldon, Phys. Rev. Lett. **113** (2014) 012502.
- [14] P.S. Hauge, S.A. Williams and G.H. Duffey, Phys. Rev. C **4** (1971) 1044.
- [15] W. von Oertzen, Eur. Phys. J. A **11** (2001) 403.
- [16] R. Bijker and F. Iachello, Nucl. Phys. A **1006** (2021) 122077 [arXiv:2011.01976].
- [17] W. von Oertzen, Nucl. Phys. A **148** (1970) 529.
- [18] W. von Oertzen and H.G. Bohlen, Phys. Rep. C **19** (1975) 1.
- [19] B. Imanishi and W. von Oertzen, Phys. Rep. **155** (1987) 29.
- [20] W. von Oertzen, Z. Phys. A **354** (1996) 37.
- [21] V. Della Rocca, R. Bijker and F. Iachello, Nucl. Phys. A **966** (2017) 158.
- [22] A.H. Santana Valdés and R. Bijker, Eur. Phys. J. Spec. Top. **229** (2020) 2353 [arXiv:2004.07872].
- [23] R. Bijker and F. Iachello, Phys. Rev. Lett. **122** (2019) 162501.
- [24] C. Wheldon et al., Eur. Phys. J. A **26** (2005) 321.
- [25] R.B. Firestone, Nucl. Data Sheets **127** (2015) 1.
- [26] M. Bouhelal, F. Haas, E. Caurier, F. Nowacki and A. Bouldjedri, Nucl. Phys. A **864** (2011) 113.

- [27] D. Mengoni, private communication.
- [28] M.A. Preston and R.K. Badhuri, Structure of the Nucleus, Addison-Wesley, Reading, Massachusetts, 1975.
- [29] S.G. Nilsson, Dan. Mat. Fys. Medd. **29** (16) (1955).
- [30] A.J. Howard, J.G. Pronko, and C.A. Whitten Jr., Phys. Rev. **184** (1969) 1094.
- [31] A.J. Howard, J.P. Allen and D.A. Bromley, Phys. Rev. **139B** (1965) 1135.
- [32] A.R. Stanford and P.A. Quin, Nucl. Phys. A **342** (1980) 283.
- [33] A. Bohr and B.R. Mottelson, Dan. Mat. Fys. Medd. **27** (16) (1953).